Geophysical Research Letters

Supporting Information for

Accuracy of ocean CO_2 uptake estimates at a risk by a reduction in the data collection

Yuanxu Dong[1,2], Dorothee C. E. Bakker[1], Peter Landschützer[3]

[1]Centre for Ocean and Atmospheric Sciences, School of Environmental Sciences, University of East Anglia, Norwich, UK; [2]GEOMAR Helmholtz Centre for Ocean Research Kiel, Kiel, Germany; [3]Flanders Marine Institute (VLIZ), Ostend, Belgium.

Correspondence to: Yuanxu Dong (ydong@geomar.de)

Contents of this file

Introduction

To make our work clearer and to help the reader better understand the main contents, we provide some supporting information below.

Text S1. Data for global ocean CO_2 flux estimates

We use the same input data as described in Landschützer et al. (2014) for the neural network training process, which are sea surface temperature (SST), sea surface salinity, chlorophyl, and mixed layer depth. The following datasets are used for estimating other variables in equation 1 of the main text. The CCI SST v2.1 (Merchant et al., 2019) is used to estimate the Schmidt number and solubility for the global ocean. The global atmospheric CO_2 fugacity (fCO_{2a}) data is calculated from the NOAA ESRL marine boundary layer CO_2 mole fraction (Dlugokencky and Tans, 2023). The quadratic wind speed (U_{10})-dependent formulation ($K_{660} = aU_{10}^2$; Ho et al., 2006; Wanninkhof, 2014) is used to calculate gas transfer velocity K_{660}. The 1° × 1°, monthly ERA5 wind speed data (Hersbach et al., 2020) from 1982 to 2020 is utilized to scale the transfer coefficient to match to a global mean K_{660} from the ^{14}C inventory method (Naegler, 2009).

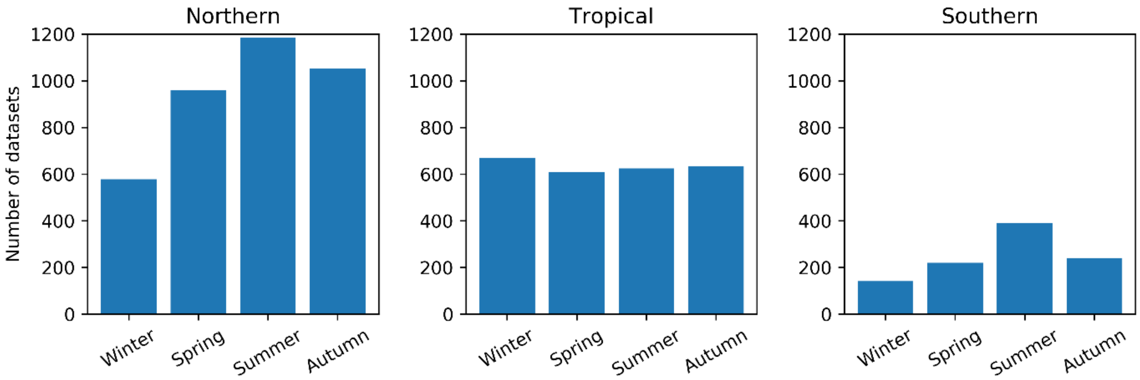

Figure S1. Seasonal distribution of the fCO_2 datasets in SOCATv2023 (Bakker et al., 2023) in the Northern, Tropical and Southern Oceans. The winter in the Northern Ocean is defined as December, January, and February, while the winter in the Southern Ocean is defined as the June, July, and August. The season in the Tropical Ocean is defined as the same in the Southern Ocean.

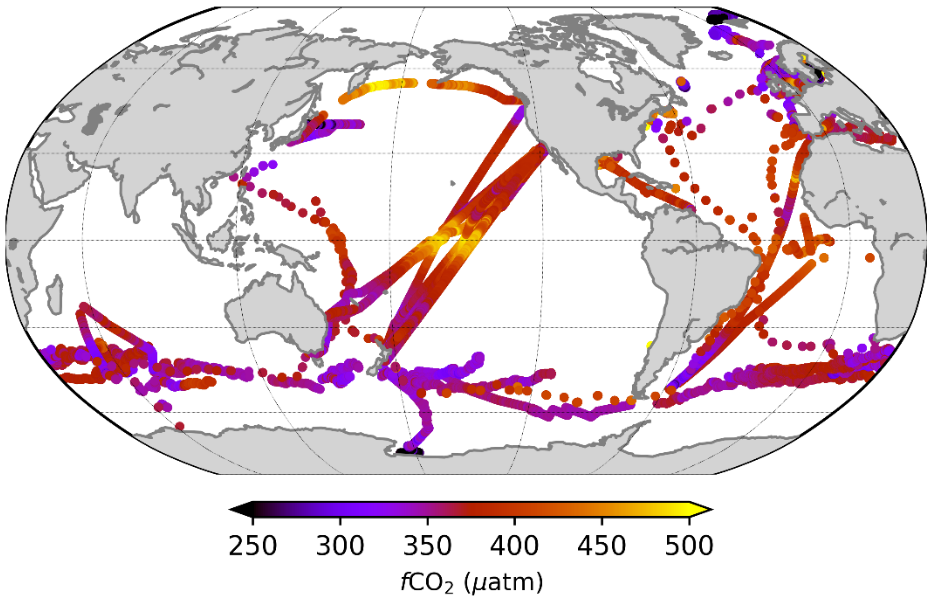

Figure S2. Global distribution of all surface water fCO_2 values (µatm) with a flag of E in SOCATv2023 (Bakker et al., 2023).

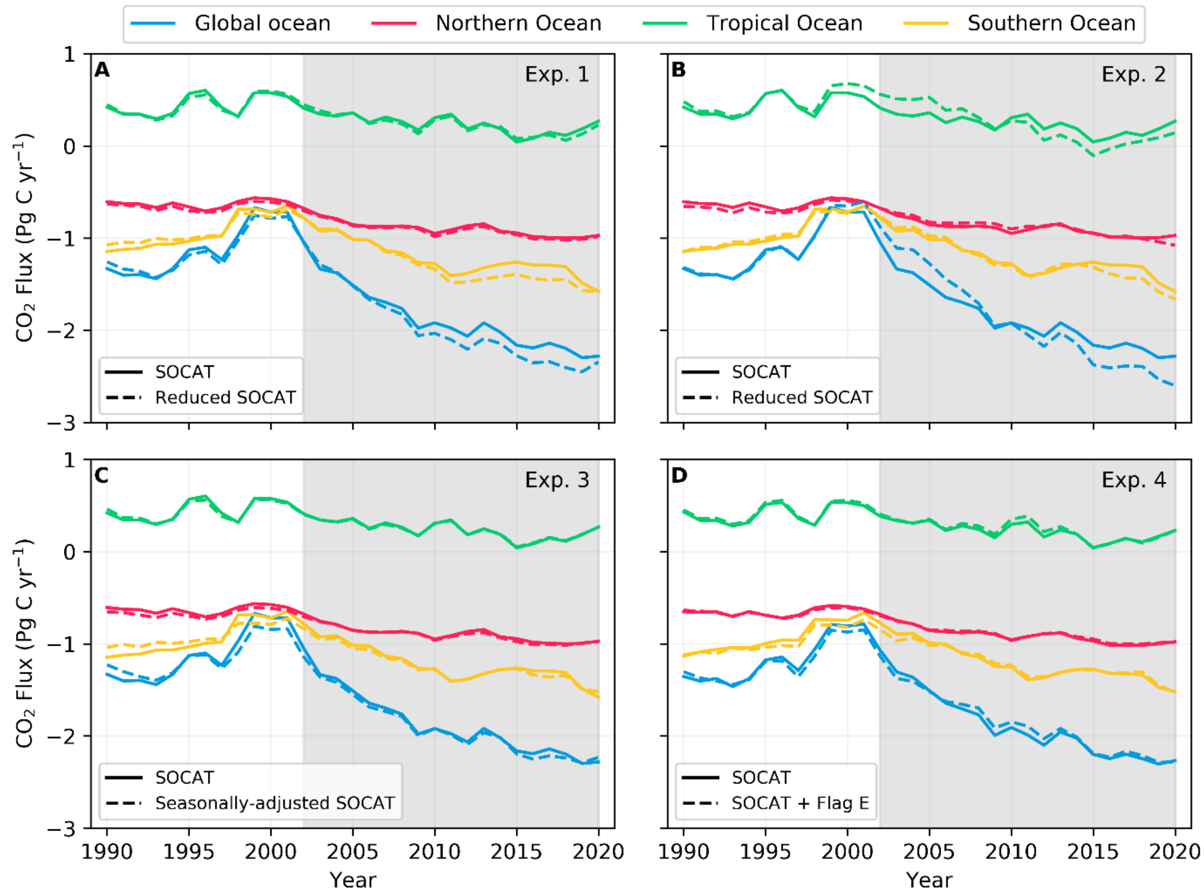

Figure S3. Global air-sea CO_2 flux estimates for 1990 to 2020 based on SOCATv2023 (solid lines) and on the four experimental datasets (dashed lines). A neural network-based method has been used to interpolate SOCAT fCO_2 to the global ocean. The blue, red, green, and yellow lines represent the flux in the global, Northern, Tropical, and Southern Oceans, respectively. Dashed lines are experimental fluxes based on SOCAT with **A**: the number of datasets reduced to a similar number as in 2020 to simulate the recent decline in the data availability; **B**: the number of datasets reduced to a similar number as in 2000 to test long-term trends; **C**: some summertime datasets removed to minimize the seasonal skew in the data; **D**: additional lower-accuracy datasets (flag of E). The unshaded and shaded area represent the phase I and phase II, respectively.

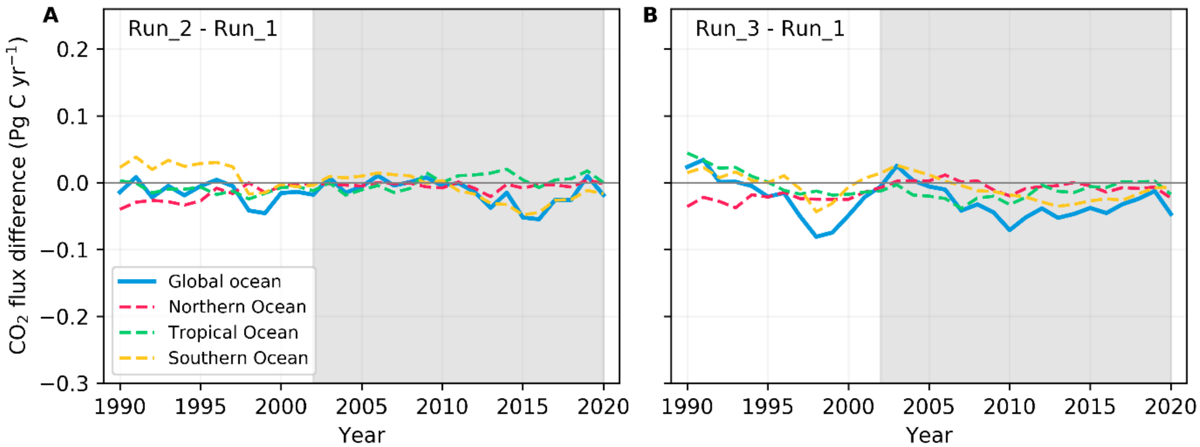

Figure S4. Differences in air-sea CO_2 flux estimates for 1990 to 2020 based on SOCATv2023 between repeat runs. The unshaded and shaded area represent the phase I and phase II, respectively.

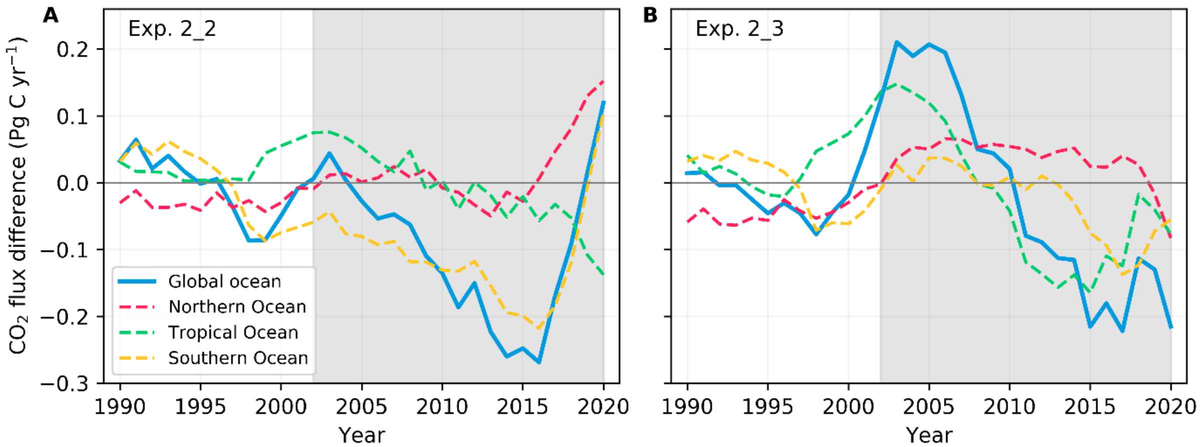

Figure S5. Differences in global air-sea CO_2 flux estimates for 1990 to 2020 between those based on the datasets in experiment 2 and those SOCATv2023 (i.e., experimental flux minus the original SOCAT-based flux). See section 2 for details. The same as experiment 2 shown in Figure 3B, but with different datasets randomly removed. The unshaded and shaded area represent the phase I and phase II, respectively.

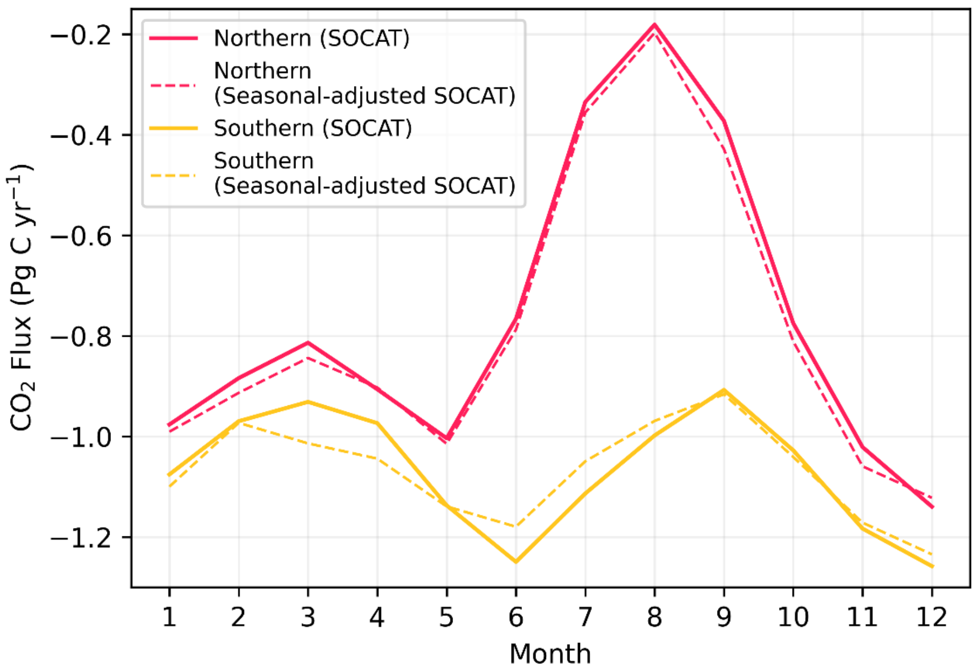

Figure S6. Air-sea CO_2 fluxes in the Northern Ocean (red) and the Southern Ocean (yellow) in each month. The fluxes shown by the solid lines are based on the gridded SOCATv2023, while the dashed lines represent the fluxes based on the seasonally adjusted SOCATv2023.

Table S1. Mean (± standard deviation, std) and trend of the global ocean air-sea CO_2 flux difference (ΔF, experimental flux minus the original SOCAT-based flux). The percentage values in the trend columns represent the trend in ΔF relative to the trend in the original SOCAT-based flux estimate (i.e., trend in ΔF / trend in F).

		Mean ± std of ΔF (Pg C yr^{-1})		Trend of ΔF (Pg C dec^{-1})	
		Phase I	Phase II	Phase I	Phase II
Exp. 1	Global	-0.018 ± 0.050	-0.092 ± 0.072	-0.097 (-16%)	-0.11 (18%)
Exp. 1	Northern	-0.030 ± 0.0078	-0.018 ± 0.0078	-0.0064 (-49%)	-0.0016 (1.2%)
Exp. 1	Tropical	-0.0013 ± 0.027	-0.011 ± 0.029	0.023 (17%)	-0.027 (20.6%)
Exp. 1	Southern	0.0134 ± 0.048	-0.062 ± 0.060	-0.11 (-25%)	-0.081 (25%)
Exp. 2	Global	0.028 ± 0.053	-0.029 ± 0.18	0.10 (17%)	-0.32 (55%)
Exp. 2	Northern	-0.034 ± 0.018	0.0087 ± 0.037	0.041 (314%)	-0.044 (33%)
Exp. 2	Tropical	0.051 ± 0.046	-0.013 ± 0.12	0.082 (61%)	-0.20 (150%)
Exp. 2	Southern	0.011 ± 0.021	-0.025 ± 0.057	-0.023 (-5.2%)	-0.084 (26%)
Exp. 3	Global	-0.027 ± 0.083	-0.029 ± 0.031	-0.21 (-35%)	0.022 (-3.8%)
Exp. 3	Northern	-0.039 ± 0.0087	-0.011 ± 0.013	0.013 (100%)	-0.0045 (3.3%)
Exp. 3	Tropical	-0.0038 ± 0.023	-0.0012 ± 0.0074	-0.036 (-27%)	0.0075 (-5.8%)
Exp. 3	Southern	0.016 ± 0.077	-0.017 ± 0.027	-0.19 (-42%)	0.019 (-5.9%)
Exp. 4	Global	-0.030 ± 0.041	0.021 ± 0.046	-0.097 (-18%)	0.027 (-4.4%)
Exp. 4	Northern	0.0068 ± 0.012	0.0064 ± 0.010	-0.026 (-69%)	0.0075 (-5.1%)
Exp. 4	Tropical	0.020 ± 0.0057	0.017 ± 0.023	-0.0014 (-1.3%)	-0.014 (11%)
Exp. 4	Southern	-0.043 ± 0.030	-0.0026 ± 0.031	-0.070 (-18%)	0.033 (-9.8%)

Reference

Bakker, D. C. E. and >100 co-authors (2023). Surface Ocean CO_2 Atlas Database Version 2023 (SOCATv2023) (NCEI Accession 0278913). NOAA National Centers for Environmental Information Dataset. https://doi.org/10.25921/r7xa-bt92. Last access 31/12/2023.

Dlugokencky, E. and Tans, P. (2023): Trends in atmospheric carbon dioxide, National Oceanic and Atmospheric Administration, Global Monitoring Laboratory (NOAA/GML), http://www.gml.noaa.gov/gmd/ccgg/trends/global.htm, last access 331/12/2022.

Ho, D. T., Law, C. S., Smith, M. J., Schlosser, P., Harvey, M., & Hill, P. (2006). Measurements of air-sea gas exchange at high wind speeds in the Southern Ocean: Implications for global parameterizations. *Geophysical Research Letters*, *33*(16). https://doi.org/10.1029/2006GL026817

Hersbach, H., Bell, B., Berrisford, P., Hirahara, S., Horányi, A., Muñoz-Sabater, J., et al. (2020). The ERA5 global reanalysis. *Quarterly Journal of the Royal Meteorological Society*, *146*(730), 1999–2049. https://doi.org/10.1002/qj.3803

Landschützer, P., Gruber, N., Bakker, D. C. E., & Schuster, U. (2014). Recent variability of the global ocean carbon sink. *Global Biogeochemical Cycles*, *28*(9), 927–949. https://doi.org/10.1002/2014GB004853

Merchant, C. J., Embury, O., Bulgin, C. E., Block, T., Corlett, G. K., Fiedler, E., et al. (2019). Satellite-based time-series of sea-surface temperature since 1981 for climate applications. *Scientific Data*, *6*(1), 1–18. https://doi.org/10.1038/s41597-019-0236-x

Naegler, T. (2009). Reconciliation of excess ^{14}C-constrained global CO_2 piston velocity estimates. *Tellus, Series B: Chemical and Physical Meteorology*, *61 B*(2), 372–384. https://doi.org/10.1111/j.1600-0889.2008.00408.x

Wanninkhof, R. (2014). Relationship between wind speed and gas exchange over the ocean revisited. *Limnology and Oceanography: Methods*, *12*(6), 351–362. https://doi.org/10.4319/lom.2014.12.351